Astron. Astrophys. 320, 399–404 (1997)

ASTRONOMY
AND
ASTROPHYSICS

Positioning the near-infrared versus optical emission peaks in NGC 1068 with adaptive optics⋆

O. Marco[1], **D. Alloin**[2], **and J.L. Beuzit**[3]

[1] Observatoire de Paris, DESPA (URA CNRS 264), F-92195 Meudon, France
[2] Service d'Astrophysique, CE Saclay (URA CNRS 2052), F-91191 Gif-sur-Yvette, France
[3] Observatoire de Grenoble (URA CNRS 708), BP 53, F-38041 Grenoble, France

Received 2 January 1996 / Accepted 22 July 1996

Abstract. The nuclear region of the Seyfert galaxy NGC 1068 has been mapped in the near-infrared, from 1.25 to 2.23 μm, with the ESO adaptive optic system COME-ON+, at a spatial resolution of about 0.5″.

Imaging was carried out in the standard J, H, K spectral bands. In addition, simultaneous imaging in the near-infrared (K band) and in the visible (I band) was performed to accurately locate the emission peaks in these two bands.

These data show the presence of strong near-infrared emission, within the central 100 pc around the nucleus. The dominant emission peak is unresolved at a resolution of about 30 pc.

The infrared (K band) emission peak is found to be offset by 0.28″ south and 0.08″ west of the optical (I band) continuum peak, and so corresponds to the location of the hidden nucleus, as defined from maser and molecular emission.

The compact infrared source, which radiates more than 66% of the near-infrared flux, appears to be associated with dust heated directly by the central active nucleus, while the extended near-infrared emission region may be related to additional local emitting processes.

We summarize in this paper the up-to-date existing tentative astrometry for NGC 1068, from UV to radio.

Key words: galaxies: NGC 1068 – galaxies: Seyfert – galaxies: nuclei of – infrared: galaxies – instruments: adaptive optics

1. Introduction

Advances in high resolution imaging from the ground, thanks to adaptive optic systems, now offer the opportunity to probe in the near-infrared the inner structure of active galactic nuclei (AGN). Indeed, these objects are extremely complex, and so far, their geometry could be inferred only indirectly. Conversely, geometrical parameters play a very important role in AGN models and therefore, their knowledge is essential. The nearest and brightest Seyfert galaxy, NGC 1068 (at a distance of 14.1 Mpc, 1″=68 pc, H_0=75 km s^{-1} Mpc^{-1}), appears as the best candidate to approach directly the AGN geometric configuration and hence to test the unification theories of AGN. The adaptive optic device COME-ON+ available at the 3.6 m telescope at ESO allows to image, in the near-infrared, bright objects such as the AGN in NGC 1068, with a spatial resolution in accordance to that achieved with the Hubble Space Telescope (HST) at visible and ultraviolet wavelengths.

The AGN in NGC 1068 has already been studied extensively. Yet, it is only recently that studies have been performed **at high angular resolution**, first in the radio range and more recently in the visible and ultraviolet windows.

The narrow line region (NLR) has a conical shape which is roughly aligned with the radio VLA or VLBI sources (Pogge, 1989, Bergeron et al., 1989). It is unclear whether the UV radiation conical shape results from intrinsically anisotropic emission or if it starts off isotropically and is collimated by an obscuring torus (Chelli et al., 1987).

Recent HST data in the visible (Evans et al., 1991, Macchetto et al., 1994) resolve the innermost part of the NLR into several distinct clouds. We follow in this paper the cloud notation by Evans et al.(1991), NLR-A to NLR-F. It is suspected from recent astrometric measurements by Capetti et al.(1995), that these clouds are anti-coincident with the 1.3 cm radio "triple" structure (Ulvestad et al., 1987).

In the near-infrared, spectroscopic imaging of the circumnuclear environment reported the brightest H_2 1-0 S(1) knot to be centered 0.3″ south-west of the near-infrared continuum peak (Blietz et al., 1994). These authors estimated the molecular density to be large enough to contribute significantly to the obscuration of the broad-line-region (BLR). Mid-infrared imaging of the narrow-line-region (Cameron et al., 1993) indicates that warm dust is associated with the narrow-line clouds and is most probably mixed with the photoionized gas. From that

Send offprint requests to: O. Marco

⋆ Based on observations collected at the European Southern Observatory, La Silla, Chile.

study it appears that the BLR extinction could be merely the result of one or a few molecular clouds on the line of sight, and it is also argued that the dust is directly heated by radiation from the central AGN source, rather than being shocked in extended star formation regions.

In the current paper, we study for the first time the distribution of the near-infrared emission at high angular resolution from adaptive optics observations of the $1.2'' \times 1.2''$ nuclear region of NGC 1068, and **the relative positions of the near-infrared and visible continuum peaks**.

2. Observations

We used the ESO 3.60-meter telescope (La Silla, Chile) and the COME-ON+ adaptive optic system (Rigaut et al. 1991, Hubin et al. 1993) on the nights 28/29 october 1993 and 5/6 november 1993 to observe in the near infrared the central region of NGC 1068.

The adaptive optics correction was performed on the brightest spot of NGC 1068 in the visible. The wavefront sensor (EBCCD after a red dichroic splitter) has a pixel size of $0.7''$ and takes into account the gravity center of the light within a $6''$ diameter circular entrance.

The detector was the SHARP (System for High Angular Resolution infrared Pictures) camera, at the f/45 Cassegrain focus, which provides an image scale of $0.05''$/pixel, resulting in a field of view of $12.8'' \times 12.8''$ (Hofmann et al. 1992).

NGC 1068 was observed in an imaging mode through the standard spectral J, H, and K bands.

Along the imaging light-path, we also performed the experiment of adding a dichroic foil to observe simultaneously in the visible (I band) with a CCD camera, and in the near-infrared (K band) with SHARP, in order to position and scale very accurately images in the two bands. The image scale for the CCD camera was $0.034''$/pixel, resulting in a field of view of $16.8'' \times 16.8''$.

During the two nights, the optical seeing measured by the ESO differential image motion monitor beside the 2.2 m telescope was not much better than $1''$. Because of this and because the visible source in NGC 1068 used to close the adaptive optics loop has a magnitude of about 12, the efficiency of the adaptive optics correction was not optimal. Therefore, the final images obtained with SHARP were not diffraction limited.

2.1. Data acquisition

In order to minimize position offsets between the calibration star and the AGN, we selected reference stars quite close to the target (within 2 degrees). For both the galaxy and the PSF reference stars, the air-mass correction was at most of 1.5, 1.97 and 1.24, for respectively the J,H and K bands.

For the J, H and K bands, we alternated object and sky imaging. We used several reference stars to derive the point spread function (PSF) for deconvolution.

For the simultaneous observations in the I and K bands, using a dichroic foil, we alternated stars and galaxy observations to track eventual flexure effects. We found these effects to be less than one pixel. We observed two different reference stars with an airmass close to that of the galaxy, in order to minimize differences of the differential refraction. All these effects are taken into account in the final errorbar determination.

We summarize in Table 1 the information about the selected data.

2.2. Data reduction

2.2.1. Infrared data reduction (J, H and K bands)

Standard infrared data reduction procedures were applied to each individual frame, for both the galaxy and the reference stars: dead pixel removal, sky subtraction, flat fielding. We also had to filter correlated noise due to the electronic output of the SHARP camera. This induces in turn a low degradation in the final angular resolution in the images, especially in the J band.

It is to be noted that the individual exposure time was chosen to provide the best possible signal-to-noise ratio for every image. Therefore, we could apply image selection according to the instantaneous seeing and retain only the frames with the best spatial resolution. For each frame we calculated the full-width-at-half-maximum (FWHM) of the object, and compared it with its value in the average image. The final number of frames retained for each filter is reported in Table 1 (columns 2 and 8). This procedure allowed us to optimize, in terms of image quality, the output of the observing sequence.

The adaptive optic system is expected to compensate for image shifting. We cross-correlated individual images to track residual shifts: the centroid coincidence between individual frames was found to be always better than 1 pixel (i.e. 0.05"). So no additional shift correction had to be applied.

Finally, a deconvolution procedure was applied using the Lucy-Richardson algorithm in the IDL package, with 30, 70 and 40 iterations for the J, H and K bands respectively. The final resolution achieved in each band is reported in Table 1.

2.2.2. Visible data reduction

All the data were reduced according to standard procedures, but no deconvolution was applied. In order to compare the I and K images, we have first determined the pixel scaling between the two bands. We used two reference stars, observed three times simultaneously in the two bands. We computed their relative offsets in the infrared band, for which we know precisely the pixel scaling. Then we made the obvious assumption that the offsets are the same in the two bands, and deduced the pixel scale of the CCD camera. We also deduced from these measurements the orientation of the field of view for the CCD camera. The pixel sizes and the FWHM are different in the two bands: therefore, the positions of the maximum peaks corresponding to the galaxy and to the reference stars were estimated by fitting 2-dimensional Gaussian profiles, using the MIDAS package. Then, for each of the I and K band, we determined the offset between the maxima of the galaxy and two reference stars, SAO 130062 and SAO 130080. We checked these results

Table 1. Parameters of the selected COME-ON+ observations

NGC 1068	Total integration time	FWHM non-deconv. N-S	FWHM non-deconv. E-W	FWHM deconvolved N-S	FWHM deconvolved E-W	Reference star	Total integration time	FWHM N-S	FWHM E-W
J (1.25 μm)	20x(40 s)	0.95″	0.95″	0.75″	0.85″	J: SAO 130075	5x(40 s)	0.65″	0.65″
H (1.68 μm)	33x(10 s)	0.65″	0.75″	0.45″	0.55″	H: SAO 130075	40x(2.5 s)	0.45″	0.45″
K (2.23 μm)	44x(3 s)	0.6″	0.7″	0.45″	0.60″	K: SAO 130075	11x(3 s)	0.45″	0.45″
I (0.8 μm)	1x(120 s)	1.4″	1.3″			I: SAO 130062	1x(5 s)	1.3″	1.3″

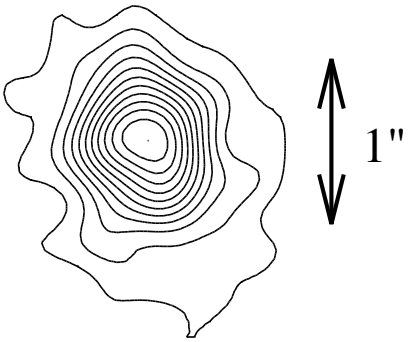

Fig. 1. Contour map of NGC 1068 in the J band with COME-ON+. The contours are linearly scaled from 10% to 100% of the peak intensity. The map is centered on the maximum peak. North is up, east to the left.

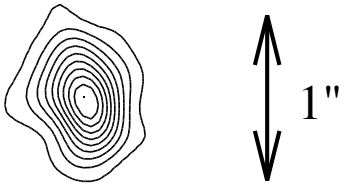

Fig. 2. Contour map of NGC 1068 in the H band with COME-ON+. The contours are linearly scaled from 10% to 100% of the peak intensity. The map is centered on the maximum peak. North is up, east to the left.

on several data sets (3 galaxy observations interlaced with 3 exposures on the 2 reference stars, always simultaneously in the two bands). We derive the error estimation from these redundant measurements.

3. Results and discussion

We present in Figs. 1, 2 and 3 the deconvolved J, H and K band images obtained with COME-ON+. Fig. 4 reports on how we calculated the offset between the near-infrared and the optical continuum peaks: the simultaneous images obtained in the visible (up) and in the near-infared (down) for the galaxy (left) and the PSF reference star (right) are presented, all centered on the PSF maximum peak.

The J, H, K near-infrared images of NGC 1068 show the nuclear emission to be extended over a 100 pc region. We do observe however in all three J, H and K bands, one dominant peak which accounts for more than 66% of the near-infrared

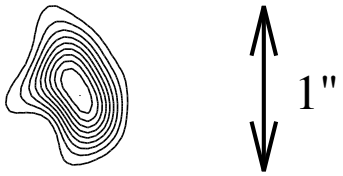

Fig. 3. Contour map of NGC 1068 in the K band with COME-ON+. The contours are linearly scaled from 10% to 100% of the peak intensity. The map is centered on the maximum peak. North is up, east to the left.

energy output of the nuclear region. Apart from the main peak, we do not isolate individual regions down to the spatial resolution of the images, but we see that the nuclear region ($1.2'' \times 1.2''$) is elongated from south-west to north-east, along an axis reminiscent of the radio emission axis (Muxlow, 1994).

3.1. Positioning the near-infrared image with respect to the visible image

Using the data acquired **simultaneously** in the K band with SHARP and the I band with a CCD camera, by means of a dichroic foil (see Sect. 2), we have computed accurately the relative positions of the maximum peaks in the two images.

The K band maximum peak is found to be located 0.28 ± 0.05 ″ south, and 0.08 ± 0.05 ″ west from the I band continuum peak. This offset along the north-south direction is about half of the spatial resolution achieved on the deconvolved image. Given the signal-to-noise ratio of the data, we are confident that such an offset is significant, although small. In NGC 1068, the I band is essentially sensitive to continuum emission, and our observed single peak in I is most probably the extension at longer wavelengths of the bright continuum source observed by Lynds et al. (1991) at 5470 Å with the HST. Indeed, we find no offset (larger than 0.05″) between the I peak on NGC 1068 and the V continuum source within NGC 1068 on which the adaptive optic loop was closed; recent measurements from V and I band HST images obtained with the WFPC2 instrument, demonstrate that the peaks in these two bands occur at the same location, within 0.05″ (Z. Tsvetanov, private communication). Within the errorbars, this position of the K peak is consistent with that found by Thatte et al. (1996, private communication): 0.41 ± 0.10 ″ south, and 0.23 ± 0.10 ″ west from the V band continuum peak.

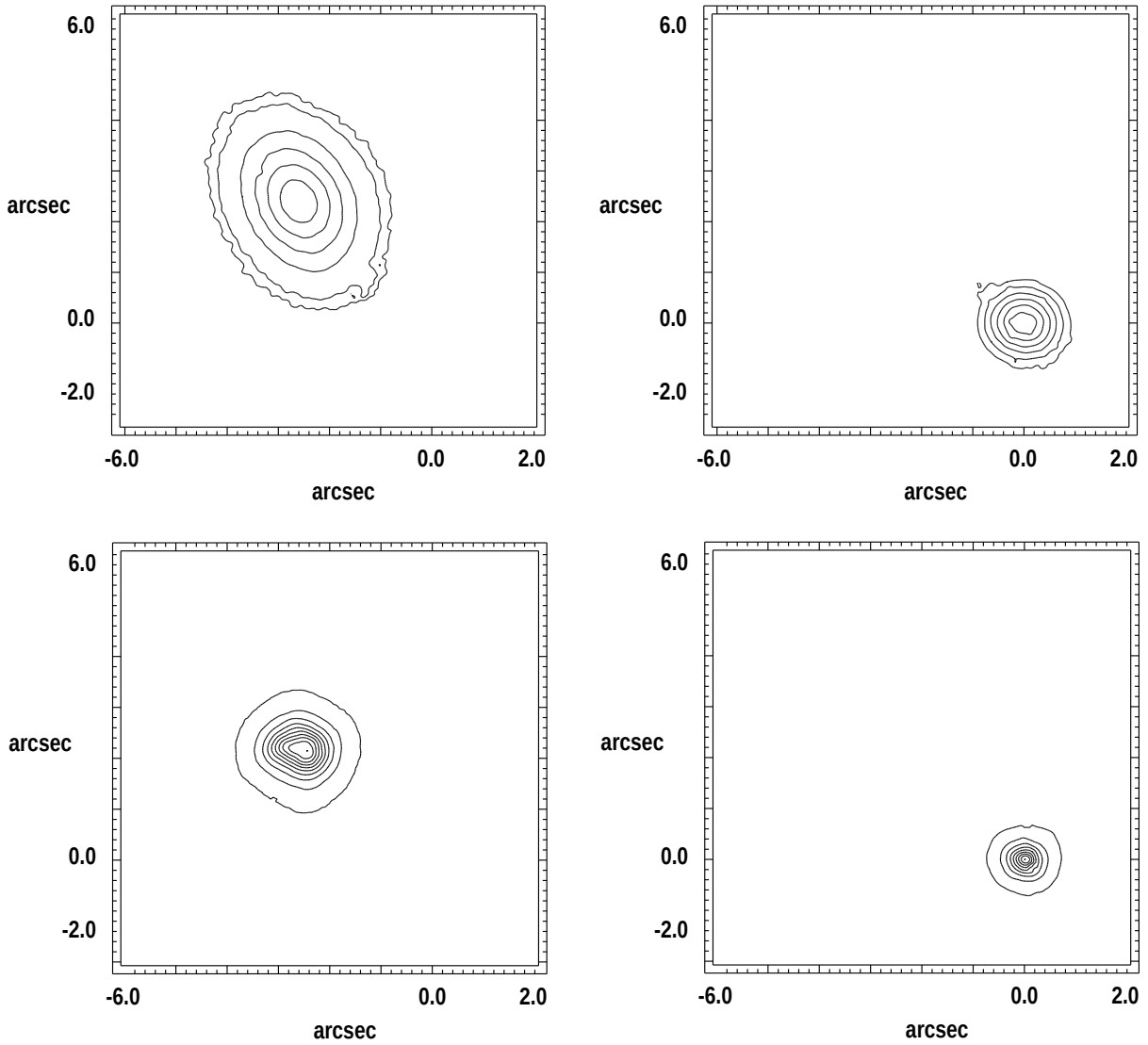

Fig. 4. Contour map of NGC 1068 (left) and the reference star SAO 130062 (right). Up: visible, Down: near-infrared (simultaneous observations). The map are centered on the reference star maximum peak. North is up, east to the left.

3.2. Identification and nature of the components within $1.2'' \times 1.2''$

Prior to any discussion regarding the nature and physics of the components (compact and extended) identified within the $1.2'' \times 1.2''$ central region of NGC 1068, as well as their relationship, it is imperative to register precisely the images at different wavelengths. This is however a quite difficult task as few precise astrometric measurements have been made so far.

In the [O III] line emission, in the visible and UV continuum emission, we rely on the HST observations (Lynds et al., 1991; Evans et al., 1991; Caganoff et al., 1991; Macchetto et al., 1994; Capetti et al., 1995). From the post-COSTAR data set (Macchetto et al., 1994), the UV and visible continuum maps have been positioned precisely, one with respect to the other, as many point like sources can be identified within the field-of-view. The UV and visible 5470 Å continuum emission peaks (which do not correspond to the true nucleus, but are scattered light from the nucleus) are found to be coincident. The 5470 Å bright continuum peak observed by Lynds et al. (1991) and corresponding also to our I band continuum peak as confirmed by the HST WFPC2 data (Sect. 3.1), is located $0.05''$ north of the [O III] NLR-B cloud and is not associated with an isolated [O III] NLR cloud. The [O III] emission peak is found within NLR-B cloud (Evans et al., 1991).

In the mid-infrared, there has been one attempt to perform astrometric measurements. The 12.4 μm peak detected by Braatz et al. (1993) has been placed by these authors with respect to the visible continuum image observed by Lynds et al. after smoothing the HST visible image to the spatial resolution of the 12.4 μm image. The 12.4 μm peak appears to be located $0.3 \pm 0.15''$ south of the emission peak in the visible (defined as the visible nucleus seen by Lynds et al.,1991). Observa-

tions at 10.3 μm by Cameron et al. (1993), although obtained with a better spatial resolution, were not intended to provide precise positioning and could only be registered, then, with "a priori" assumptions: using a cross-correlation technic, the 10.3 μm peak was found to be roughly coincident with NLR-C cloud. Recent observations with adaptive optics at 3.5 μm and 4.8 μm (Marco et al., 1997), indicate that the peak emission at these wavelengths is located 0.3″ south of the visible peak, that is at the same place as the 12.4 μm peak (Braatz et al., 1993), and the 2.2 μm peak (Sect. 3.1). Therefore, it is most probable that the 10.3 μm peak is at this same position. Simultaneous imaging in the 10 μm window and in the visible would confirm this guess.

In the radio range, a detailed discussion has been provided by Gallimore et al. (1996c), based upon new measurements of the maser positions and kinematics. These authors question the previous correspondence established by Evans et al. (1991) between the radio and the [O III] line emission maps. We shall adopt hereafter the new alignment proposed by Gallimore et al. (1996c) having the radio component S1, in the southern complex (Gallimore et al., 1996a), almost coincident with the 12.4 μm peak (Braatz et al., 1993), the UV polarization center (Capetti et al., 1995), and thought to locate the hidden true nucleus.

Building up from these results and using our precise relative positions of the K and (I≡V) band images we are led to the sketch shown on Fig.5, where our near-infrared data have been overlaid on the [O III] HST image, and compared with other waveband data.

What is the relevance of the near-infrared K peak to the true nucleus, and which signatures do we expect from this nucleus? Since the observations in polarized light of broad permitted lines from the nuclear region by Antonucci & Miller (1985), the presence of a very thick dust/molecular parsec-scale absorbing torus, around the central engine, has been suspected. The location of the "true" nucleus has been argued on the basis of:

(i) its energetic radiation: the apex of the ionizing cone from the [O III] line emission distribution (Pogge, 1988, Evans et al., 1991),
(ii) its dust/molecular component: location of the water megamaser (Gallimore et al., 1996 c),
(iii) its polarization properties: the pattern of the UV polarization vectors (Capetti et al., 1995).

Following Gallimore et al. (1996 a,b,c), who discuss all these arguments, the "true" nucleus is found to be most likely located south of NLR-A cloud, and 0.3″ south of the visible peak (Lynds et al., 1991), close to the mid-infrared 12.4 μm peak.

This mid-infrared emission at 12.4 μm is quite consistent with emission of grains at a temperature between 200-500 K. As the 2.2 μm emission peak is roughly coincident with the 12.4 μm source, it is a reasonable assumption that the 2.2 μm compact emission is also due to hot dust (T_{dust} ≈1000 K) heated directly by the true nucleus.

What is the nature of the extended near-infrared emission in K? The relation between the temperature of the grains heated directly by the nuclear source, and their distance from the nucleus, assuming an average grain size of 0.05 μm, is given by:

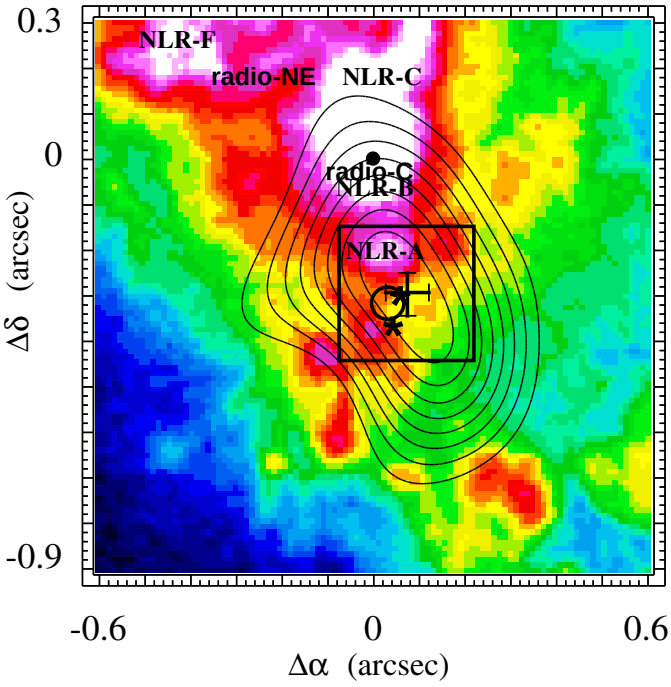

Fig. 5. Contour map of NGC 1068 in the K band (linearly scaled from 10% to 100% of the peak intensity), overlaid on an image from the HST in the [O III] line (Macchetto et al., 1994). We show the [O III] line NLR-clouds as identified by Evans et al. (1991), the radio sources NE & C as positioned by Gallimore et al. (1996c). North is up, east to the left. Symbols are: **dot** : the continuum peak at 5470 Å (Lynds et al., 1991), also our I peak (V and I being located at the same position, according to Z. Tsvetanov, 1996); **stars** : the radio components S1 and S2 as located by Gallimore et al. (1996c); **box** (size indicates errorbar): the 12.4 μm peak positioned by Braatz et al. (1993); **cross** (size indicates errorbar): the K near-infrared peak as positioned in this paper; **circle** (size indicates errorbar): the symmetry center of the UV/optical polarization (Capetti et al., 1995).

$$R = 0.14 \left(\frac{L}{1.5 \times 10^{11} L_{\odot}} \right)^{0.5} \left(\frac{T}{1500\,K} \right)^{-2.8} \text{ parsecs}$$

where L is the observed optical/UV luminosity of the continuum source (estimated to $1.5 \times 10^{11} L_{\odot}$), and T the dust temperature (Cameron et al., 1993).

This means that dust located at ≈40 pc will be heated to about 200 K. Even for grains with lower emissivities and/or with smaller sizes, the temperature will not go above ≈350 K. Indeed, Tresch-Fienberg et al. (1987) who measured color temperatures for the overall nuclear region have found a maximum temperature at 415 K. With such a temperature, the dust contribution at about 2.2 μm would likely be minor and stellar emission would be dominant. So, in the extended near-infrared emission region, either hot dust is not the only emitting process at 2.2 μm, or there are secondary local heating sources which con-

tribute in heating dust at a higher temperature. It is known already that the 10.3 μm emission in the nuclear region is associated with narrow-line emission (Cameron et al., 1993), and this indicates that warm dust is intimately mixed with photoionized gas clouds. Radiation from young hot stars in clusters would be a natural explanation for the gas ionisation and excitation, and for the heating of the surrounding dust and molecular material they originated from. The proximity of the outflowing radio jet and the presence of large quantities of material might have been favorable factors for star formation in this region.

4. Conclusion

The use of the COME-ON+ adaptive optics has allowed us to image the nucleus of NGC 1068 in the near-infrared with an improved resolution. These new results are in agreement with and extend the results of previously published data sets in the near-infrared. They can be interpreted in the light of complementary data sets collected at UV, visible and mid-infrared wavelengths, with comparable spatial resolutions. The following results are to be underlined:

1. By observing simultaneously through the K and I bands, we have determined that the K emission peak is offset to the south by $\approx 0.30''$ with respect to the continuum I peak.

2. Building up from this precise location of the K band image relative to the I band image and taking advantage of the improved spatial resolution of the adaptive optic observations, we have complemented the relative registration of the $1.2'' \times 1.2''$ central region of NGC 1068 at near infrared wavelengths with those already performed at radio, visible and UV wavelengths. The K emission peak is found to be located at the position of the true hidden nucleus.

3. The near-infrared peak relates largely to dust heated directly by the emission from the hidden nucleus.

4. The extended near-infrared emission region should host some additional and local dust heating or it is related to other emission processes.

5. Improvements of our understanding of the AGN in NGC 1068 requires precise astrometry so that the various sources observed, thanks to the high spatial resolution achieved with the HST in the ultraviolet and the visible and with adaptive optics in the near-infrared, can be placed in exact correspondence. In particular, work at 5 and 10 μm , the most favorable region for the direct detection of the torus, should be performed in an extensive way.

Acknowledgements. We warmly thank Z. Tsvetanov who provided us with timely HST WFPC2 results. We are particularly grateful to Dr. Bonaccini, Gendron, Genzel, Quirrenbach and Thatte, for enlightening discussions about the adaptive optic performances. We acknowledge as well interesting comments by J.Christou, J.P.Veran and O.Lai on the use of deconvolution algorithms.

References

Antonucci, R.R.J., Miller, J.S., 1985, ApJ, 297, 621
Antonucci, R.R.J., 1992, in Testing the AGN Paradigm, eds. S.S. Holt, S.G. Neff, C.M. Urry (New York: AIP), AIP Conference Proceedings, Vol. 254, 486
Antonucci, R.R.J., Hurt, T., Miller, J.S., 1994, ApJ, 430, 210
Bergeron, J., Petitjean, P., Durret, F., 1989, A&A, 213, 61
Blietz, M., Cameron, M., Drapatz, S., et al., 1994, ApJ, 421, 92
Braatz, J.A., Wilson, A.S., Gezari, et al., 1993, ApJ, 409, L5
Caganoff, S., Antonucci, R.R.J., Ford, H.C., et al., 1991, ApJ, 377, L9
Cameron, M., Storey, J., Rotaciuc, et al., 1993, ApJ, 419, 136
Capetti, A., Axon, D.J., Macchetto, F., Sparks, W.B., Boksenberg, A., 1995, ApJ, 446, 155
Capetti, A., et al., 1995, ApJ, 452, L87
Chelli, A., Perrier, C., Cruz-Gonzáles, I., Carrasco, L., 1987, A&A, 177, 51
Claussen, M.J., Lo, K.Y., 1986, ApJ, 308, 592
Code, A.D., et al., 1993, ApJ, 403, L63
Evans, I.N., Ford, H.C., Kinney, A.L., et al., 1991, ApJ, 369, L27
Gallais, P., 1991, "L'activité dans les régions centrales de galaxies: l'apport de l'imagerie infrarouge entre 1 et 5 microns" PhD thesis, University of Paris 7
Gallimore, J.F., Baum, S.A., O'Dea, C.P., Pedlar, A., 1996a, ApJ, 458, 136
Gallimore, J.F., Baum, S.A., O'Dea, C.P., Brinks, E., Pedlar, A., 1996b, ApJ 462, 740
Gallimore, J.F., Baum, S.A., O'Dea, C.P., 1996c, ApJ 464, 198
Hofmann R., Blietz M., Duhoux P., et al., 1992, In: Ulrich M.-H. (ed), Progress in Telescope and Instrumentation Technologies, ESO, Garching, 687
Hubin, N., Rousset, G., Beuzit, J.L., et al., 1993, Messenger 71, 50
Krabbe, A., Sternberg, A., Genzel, R., 1994, ApJ, 425, 72
Léna P., "Astrophysics with adaptive optics: results and challenges", Adaptive optics for astronomy, NATO-ASI, Ed. D. Alloin and J.-M. Mariotti, Kluwer, 1994
Lynds, R., Faber, S.M., Groth, E.J., et al., 1991, ApJ, 369, L31
Macchetto, F., Capetti, A., Sparks, W.B., 1994, ApJ, 435, L15
Marco, O., Alloin, D., Lacombe, F., et al., 1997, A&A, in preparation
Miller, J.S., Antonucci, R.R.J., 1983, ApJ, 271, L7
Moorwood, A.F.M., Oliva, E., 1993, "Infrared spectroscopy of starburst and Seyfert galaxies", CIRP5: Topical Conference on infrared astrophysics, Infrared Physics, ed. Kneubuhl
Muxlow, T.W.B., 1994, in *Sub-arcsecond Radio Astronomy*, Cambridge University Press, eds. R.J. Davis & R.S. Booth, 252
Planesas, P., Scoville, N., Myers, S.T., 1991, ApJ, 369, 364
Pogge, R.W., 1988, ApJ, 328, 519
Pogge, R.W., 1989, ApJ, 345, 730
Rigaut, F., Rousset, G., Kern, P., et al., 1991, A&A, 250, 280
Rotaciuc, A., Krabbe, A., Cameron, et al., 1991, ApJ, 370, L23-26
Rousset G., Beuzit J.-L., Hubin N., et al., "The Come-On-Plus Adaptive Optics System : Results and performance", ICO conference on Active and Adaptive Optics, Garching (Germany), August 2-5, (1993)
Tacconi, L.J., Genzel, R., Blietz, et al., 1994, ApJ, 426, L77
Tresch-Fienberg, R., Fazio, G.G., Gezari, D.Y., et al., 1987, ApJ, 312, 542
Ulvestad, J.S., Neff, S.G., Wilson, A.S., 1987, AJ, 92, 22.

This article was processed by the author using Springer-Verlag LaTeX A&A style file *L-AA* version 3.